PCB Rogowski Coil Array With Discrete Electrostatic Shielding for Current Measurement of Paralleled Chips in Power Devices

Yongfan Zhan, Ganyu Feng, Jia Wan, Xuebao Li, *Member, IEEE*, Rui Jin, *Member, IEEE*, Peng Sun, Zhibin Zhao, *Member, IEEE*, and Xiang Cui, *Senior Member, IEEE*

***Abstract*—A printed circuit board (PCB) Rogowski coil array is capable of measuring the currents of the paralleled chips inside power devices; the operating status and failure behavior of power devices may thus be monitored. The conventional continuous electrostatic shielding provides immunity to capacitive coupling interference for the PCB Rogowski coil array but fails to suppress inductive coupling interference. Equivalent circuit models of the PCB Rogowski coil array with continuous electrostatic shielding are established and the influence mechanism of the inductive coupling interference on the Rogowski coil array is analyzed in this article. The symmetry of the inductive coupling interference components is discovered in the waveforms from the PCB Rogowski coil array with continuous electrostatic shielding. This article proposes a discrete electrostatic shielding structure for the PCB Rogowski coil array, which is validated through switching experiments to have immunity against both capacitive and inductive coupling interference. The PCB Rogowski coil array with discrete electrostatic shielding proposed in this article can be used for research works on paralleled chips of power devices, thus providing a foundation for condition monitoring and design optimization of power devices.**

***Index Terms*—Current measurement, electrostatic shielding, inductive coupling interference, power device, Rogowski coil.**

I. Introduction

POWER devices such as IGBTs are the essential components of power transformation equipment and electric vehicles [1], [2]. In order to increase the current capacity of power devices, multiple power chips connected in parallel are generally arranged inside them [3], [4]. The paralleled chips suffer from a current distribution imbalance, which is influenced by conditions such as chip parameters and package parasitic parameters [5], [6], [7], [8]. Excessive current in some of the chips may lead to chip failure, which in turn causes the failure of the whole device [9], [10]. Therefore, measuring the current distribution among internal chips is of great significance to improve the reliability of the device.

Compared with other current measurement methods, such as current sensing resistors [11], [12], current transformers [13], and Hall effect current sensors [14], [15], Rogowski coils offer the advantages of wide bandwidth, galvanic isolation, small size, temperature stability, etc [16]. Even though they are unable to measure dc components [17], Rogowski coils have been widely applied in current measurement scenarios in power electronics since most of the relevant current waveforms, such as for semiconductor switches, are discontinuous and the zero level is readily identified [18], [19]. For example, the wire-wound Rogowski coils were designed and mounted on the busbars inside an IGBT module to obtain the transient current distribution of two paralleled IGBT chips in the module [20]. Another example is that the Rogowski coils wound on rectangular formers with a bandwidth of 5 kHz to 1.3 MHz were mounted on the emitter pillar inside a press-pack IGBT device, and the current waveforms of three parallel-connected IGBT chips were obtained [21].

Unlike wire-wound Rogowski coils, printed circuit board (PCB) Rogowski coils have advantages such as ease of manufacturing, good consistency, and low cost, and have also been widely used for current measurement in power electronics [22], [23]. For example, a rectangular PCB Rogowski coil was designed and installed near the emitter plate of an IGBT power device to monitor the device current and provide short circuit protection [24]. Two circular PCB Rogowski coils were mounted on the emitter bonding wires of two chips in an IGBT module to measure the chip currents [25]. In order to measure more currents of paralleled chips inside a power device, a compact embedded Rogowski coil array had been proposed [26]. The Rogowski coil array with 10 optimized rectangular Rogowski coils on a PCB substrate had been developed, and the top layer copper and bottom layer copper of the PCB were utilized as electrostatic shieldings [27]. The same technique was also applied to a 4.5 kV Press Pack IGBT power device and an 18 kV SiC IGBT power device to characterize the current sharing among multiple paralleled chips [28].

It is known that the switching operations of power devices generate time-varying electric field and magnetic field in space simultaneously, which may lead to measurement errors of

Manuscript received 26 January 2024; revised 4 April 2024; accepted 20 April 2024. Date of publication 24 April 2024; date of current version 20 June 2024. This work was supported by the State Grid Corporation Technology Project under Grant 5500-202399662A-3-2-ZN. Recommended for publication by Associate Editor M. Shen. *(Corresponding author: Xuebao Li.)*

Yongfan Zhan, Ganyu Feng, Jia Wan, Xuebao Li, Peng Sun, Zhibin Zhao, and Xiang Cui are with the State Key Laboratory of Alternate Electrical Power System with Renewable Energy Sources, North China Electric Power University, Beijing 102206, China (e-mail: zhanyongfan@ncepu.edu.cn; 120232101125@ncepu.edu.cn; 120212201404@ncepu.edu.cn; lxb08357x@ncepu.edu.cn; sunpeng@ncepu.edu.cn; zhibinzhao@ncepu.edu.cn; x.cui@ncepu.edu.cn).

Rui Jin is with the Beijing Institute of Smart Energy, Huairou Laboratory, Beijing 102209, China (e-mail: jinrui@bise.hrl.ac.cn).

Color versions of one or more figures in this article are available at https://doi.org/10.1109/TPEL.2024.3392937.

Digital Object Identifier 10.1109/TPEL.2024.3392937

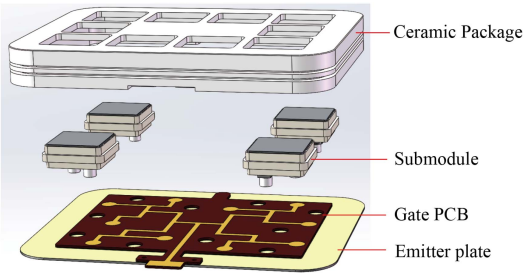

Fig. 1. Press-pack IGBT power device with four paralleled IGBT chips.

Rogowski coils [29]. Hence, the Rogowski coils should have the immunity to both capacitive coupling interference and inductive coupling interference simultaneously. For a single Rogowski coil, capacitive coupling interference may be suppressed by electrostatic shielding, while a return conductor balances vertical magnetic flux linkage thus inductive coupling interference may also be suppressed [30], [31]. Taking PCB Rogowski coil as an example, the grounded copper layers above and below the Rogowski coil guide capacitive coupling interference currents to flow into ground [32]. However, for PCB Rogowski coil arrays with conventional continuous electrostatic shielding (CES), though capacitive coupling interference may be suppressed by CES, inductive coupling interference introduced by multiple signal channels cannot be suppressed. In order to solve this problem, PCB Rogowski coil array with discrete electrostatic shielding (DES) is proposed in this article, which have the immunity to both capacitive coupling interference and inductive coupling interference.

The rest of this article is organized as follows. In Section II, a press-pack IGBT power device and a PCB Rogowski coil array with CES are introduced. The analysis of the inductive coupling interference is given based on equivalent circuits of the Rogowski coil array. In order to suppress the inductive coupling interference, a PCB Rogowski coil array with a novel DES structure is proposed in Section III. The current waveforms of paralleled chips inside the IGBT power device, which are measured by the PCB Rogowski coil arrays with different shielding structures are presented and discussed in Section IV. Finally, Section V concludes this article.

II. PCB Rogowski Coil Array With CES

A. IGBT Power Device and PCB Rogowski Coil Array

A press-pack IGBT power device is illustrated in Fig. 1. The power device consists of a ceramic package, a gate connection PCB, an emitter plate, and several submodules. The device supports a variable number of submodules. Each submodule contains one IGBT chip. The top side of the submodule corresponds to the collector electrode of the IGBT chip, while the two terminals at the bottom correspond to the gate and emitter electrodes of the IGBT chip, respectively.

In order to characterize the current distribution of the paralleled chips inside the device, a PCB Rogowski coil array with CES was developed. The coil array can be divided into the coil part and the signal output part from an appearance perspective,

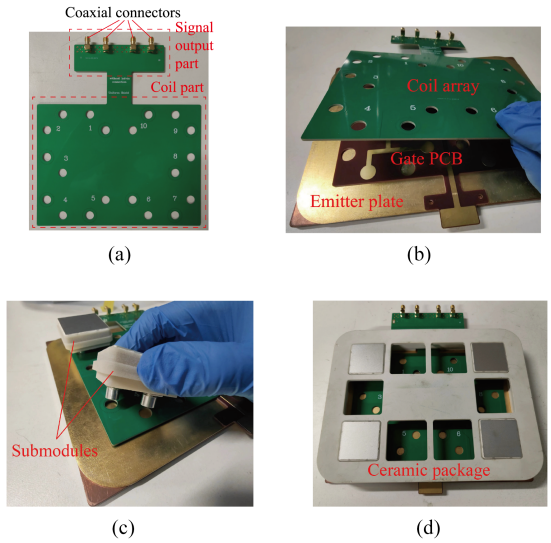

Fig. 2. Way to integrate the coil array into the IGBT device. (a) Appearance of the coil array. (b) Assembly of the coil array. (c) Assembly of the submodules. (d) Assembly of the ceramic package.

as shown in Fig. 2(a). The coil part has ten PCB Rogowski coils, and the signal output part has ten coaxial connectors. Each Rogowski coil corresponds to the emitter terminal of a submodule, thereby enabling measurement of the chip currents inside the IGBT power device. Each Rogowski coil is connected to a corresponding coaxial connector for signal output.

The way to integrate this PCB Rogowski coil array into the power device is shown in Fig. 2. First, the PCB Rogowski coil array is placed above the emitter plate and the gate PCB of the device. Several single-chip submodules are then placed in the slots, with the terminals of the submodules passing through the Rogowski coils. Finally, a ceramic package is used to fix the positions of the submodules. If necessary, silicone rubber can be used to bond the ceramic package and the emitter plate together. When the device is assembled as a whole, the coil part of the coil array is packaged inside the device, and the signal output part of the coil array protrudes outside the ceramic package through a notch.

The perspective view of the PCB Rogowski coil array with CES is shown in Fig. 3(a). The coil array is implemented on a 6-layer PCB. The Rogowski coils are arranged from the second signal layer to the fifth signal layer of the PCB, consisting of PCB traces and vias. The 1st and 6th layers of the PCB have grounded copper planes as electrostatic shielding, as shown in Fig. 3(b). The electrostatic shielding is continuous, completely covering the entire coil array. The structure of the PCB Rogowski coil array is basically consistent with former research as [27].

Rogowski coils and integrators are always found in pairs in current measurement scenarios [22]. The Rogowski coil is based on the law of electromagnetic induction. In a certain frequency range, the output voltage v_c of a Rogowski coil is proportional to the rate of change of the current under test, as shown in the following:

$$v_c = M_c \frac{\mathrm{d}i_m}{\mathrm{d}t} \tag{1}$$

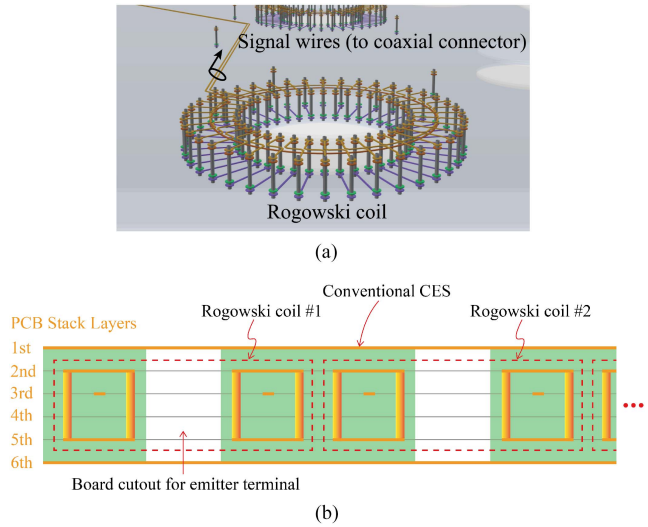

Fig. 3. Structure of the PCB Rogowski coil array with CES. (a) Perspective view of a coil. (b) Cross section of the coil array.

where M_c is the mutual inductance between the Rogowski coil and the current-carrying conductor, and i_m is the current under test. Such a signal cannot directly characterize the current, so an integrator is connected to the Rogowski coil to transform the signal. In a certain frequency range, the output voltage vint of the integrator satisfies

$$v_a = \frac{1}{T_1}\int v_c \mathrm{d}t = \frac{M_c}{T_1} i_m \tag{2}$$

where T_1 is the time constant of the integrator. The coefficient M_c/T_1 is the transformation ratio between the integrator output voltage and the current under test, and also the sensitivity of the Rogowski current sensor.

The CES of the PCB Rogowski coil array is grounded by connecting to the outer conductors of the coaxial cables since the outer conductors of the oscilloscope's input ports are typically grounded through the power cord of the oscilloscope. Therefore, the current of capacitive coupling interference may flow to ground through the CES and the oscilloscope without affecting the measurements of the Rogowski coils.

Although capacitive coupling interference is suppressed by the CES, inductive coupling interference still affects the current measurement system. The outer conductors of the coaxial cables connect via the CES at one end, and the oscilloscope ground at the other end, forming multiple loops. Time-varying magnetic field generated by the power device induces currents within these loops. This leads to discrepancies between the coil outputs and the voltage signals acquired by the oscilloscope. To analyze the impacts of such inductive coupling on measurement, further investigation is provided as follows.

B. Analysis of the Inductive Coupling Interference

The outer conductors of the two coaxial cables in Fig. 4 may be modeled as a loop. Consider a conductor loop c_1 in a time-varying magnetic field, as illustrated in Fig. 5. Point G is the reference potential point on the loop. A current $i(t)$ is induced in

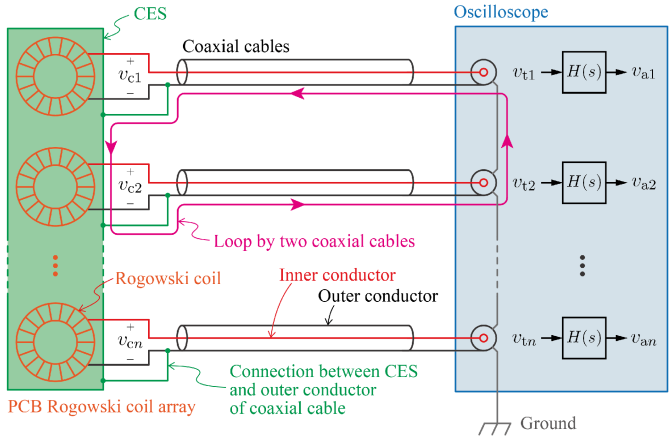

Fig. 4. Schematic diagram of the current measurement system by using the PCB Rogowski coil array with CES.

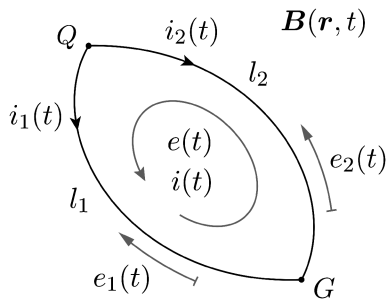

Fig. 5. Conductor loop in a time-varying magnetic field.

the loop due to electromagnetic induction. The current satisfies

$$L\frac{\mathrm{d}i(t)}{\mathrm{d}t} + Ri(t) = e(t) \tag{3}$$

and the solution of the equation is

$$i(t) = \exp(\lambda t)\left[i(t_0) + \int_{t_0}^{t} \frac{\exp(-\lambda\tau)}{L} e(\tau)\mathrm{d}\tau\right], t > t_0 \tag{4}$$

where $e(t)$ is the total induced electromotive force in the loop, $\lambda = -R/L$ is the eigenvalue of the loop current equation, R is the total resistance of the loop, and L is the inductance of the loop.

The total induced electromotive force $e(t)$ obeys Faraday's law of electromagnetic induction as (5), where $\boldsymbol{E}$ is the induced electric field from the time-varying magnetic field, S represents a surface enclosed by the loop c_1, with $d\boldsymbol{S}$ and $d\boldsymbol{l}$ forming a right-hand-grip relationship. The induced current $i(t)$ has the same reference direction as $e(t)$

$$e(t) = \oint_{c_1} \boldsymbol{E}(\boldsymbol{r},t)\cdot \mathrm{d}\boldsymbol{l} = -\frac{\mathrm{d}}{\mathrm{d}t}\int_S \boldsymbol{B}(\boldsymbol{r},t)\cdot \mathrm{d}\boldsymbol{S}. \tag{5}$$

Assume that point G and any point Q divide the loop into two conductor segments l_1 and l_2. Each conductor segment has its own induced electromotive force, resistance, and inductance. The electromotive forces of the conductor segments may be

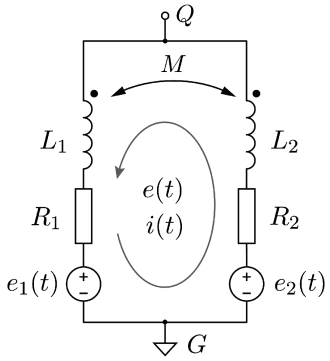

Fig. 6. Circuit model of the conductor loop.

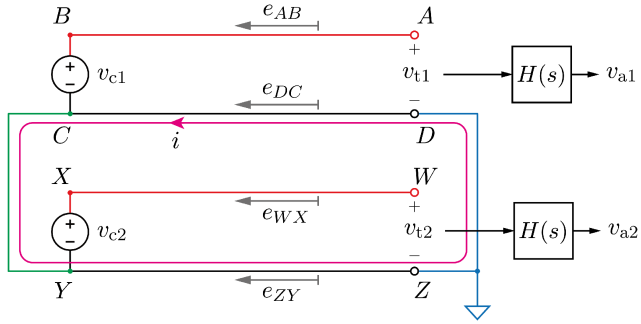

Fig. 7. Model of two Rogowski coils with CES.

expressed as

$$e_1(t) = \int_{l_1:G\to Q} \boldsymbol{E}(\boldsymbol{r},t)\cdot \mathrm{d}\boldsymbol{l} \tag{6}$$

$$e_2(t) = \int_{l_2:G\to Q} \boldsymbol{E}(\boldsymbol{r},t)\cdot \mathrm{d}\boldsymbol{l}. \tag{7}$$

The inductance of loop c_1 may be determined through the energy method [33]. Assuming a current i exists in the loop and the total magnetic energy in space is W_m, then the inductance of the loop may be determined as

$$L = \frac{2W_\mathrm{m}}{i^2}. \tag{8}$$

The inductance of conductor segments l_1 and l_2 may be determined utilizing the same method. Taking l_1 as an example. Assuming in space there exists only conductor l_1 with current i_1 flowing through it, the magnetic energy in space is $W_{\mathrm{m}1}$, then the inductance of the conductor may be determined as

$$L_1 = \frac{2W_{\mathrm{m}1}}{i_1^2}. \tag{9}$$

As for the mutual inductance between the two conductors l_1 and l_2, we first assume the two conductors in the system are standalone (not connected). The relationship between the total magnetic energy and the inductance of conductors is given by

$$\begin{aligned} W_\mathrm{m} &= \frac{1}{2}[i_1 \quad i_2]\begin{bmatrix} L_1 & M \\ M & L_2 \end{bmatrix}\begin{bmatrix} i_1 \\ i_2 \end{bmatrix} \\ &= \frac{1}{2}L_1 i_1^2 + \frac{1}{2}L_2 i_2^2 + M i_1 i_2 \end{aligned} \tag{10}$$

where the mutual inductance M between the two conductor segments may be therefore determined by

$$M = \frac{1}{i_1 i_2}\left(W_\mathrm{m} - \frac{1}{2}L_1 i_1^2 - \frac{1}{2}L_2 i_2^2\right). \tag{11}$$

Based on (8)–(11), the loop c_1 with two points G and Q in a varying magnetic field may be modeled as a lumped circuit composed of voltage sources, resistances, and inductances, as shown in Fig. 6. Therefore, the potential at point Q may be obtained by calculations in the lumped circuit as

$$\begin{aligned} \varphi_Q(t) &= e_1(t) + R_1 i(t) + (L_1 - M)\frac{\mathrm{d}i(t)}{\mathrm{d}t} \\ &= [e_2(t) - e(t)] + (R - R_2)i(t) \\ &\quad + [L - (L_2 - M)]\frac{\mathrm{d}i(t)}{\mathrm{d}t} \\ &= e_2(t) - R_2 i(t) - (L_2 - M)\frac{\mathrm{d}i(t)}{\mathrm{d}t} \\ &\quad - \left[e(t) - Ri(t) - L\frac{\mathrm{d}i(t)}{\mathrm{d}t}\right] \\ &= e_2(t) - R_2 i(t) - (L_2 - M)\frac{\mathrm{d}i(t)}{\mathrm{d}t} \end{aligned} \tag{12}$$

where R_1 is the resistance of the conductor l_1, and R_2 is the resistance of the conductor l_2. The inductances satisfy $L = L_1 + L_2 - 2M$. The total induced electromotive force of the loop $e(t)$ and the electromotive forces of the conductor segments satisfy $e(t) = e_2(t) - e_1(t)$.

Equation (12) provides the approach for calculating the potential at any point on a conductor loop in a time-varying magnetic field. It is indicated that the potentials at points on a grounded conductor loop in a time-varying magnetic field are not identically zero.

The analysis of the inductive coupling interference starts with two Rogowski coils as shown in Fig. 7. The Rogowski coils are simplified as voltage sources $v_{\mathrm{c}1}$ and $v_{\mathrm{c}2}$. The inner and outer conductors of the coaxial cable are modeled as conductor segments, respectively. The CES and the oscilloscope ground are considered as two equipotential bodies since their dimensions are much smaller than the length of the coaxial cables, that is, node C and node Y have the same potential, node D and node Z have the same potential. Therefore, the loop $DCYZ$ may be regarded as a grounded conductor loop as described above.

There are corresponding induced electromotive forces on each conductor segment due to the time-varying magnetic field from the power device, and current i is induced in the loop consisting of nodes $DCYZ$. The voltage signal $v_{\mathrm{t}1}$ at the end of the coaxial cable may be expressed as

$$\begin{aligned} v_{\mathrm{t}1} &= \varphi_A - \varphi_D \\ &= (\varphi_B - e_{AB}) - \Big[(\varphi_C - e_{DC}) \\ &\quad + R_{DC} i + (L_{DC} - M_{DC\text{-}YZ})\frac{\mathrm{d}i}{\mathrm{d}t}\Big] \end{aligned}$$

$$= (\varphi_B - \varphi_C) - (e_{AB} - e_{DC}) - \left[R_{DC} i + (L_{DC} - M_{DC\text{-}YZ}) \frac{\mathrm{d}i}{\mathrm{d}t}\right] = v_{\mathrm{c}1} - \left[R_{DC} i + (L_{DC} - M_{DC\text{-}YZ}) \frac{\mathrm{d}i}{\mathrm{d}t}\right] \tag{13}$$

where φ represents node potentials, $e_{AB} = \int_{\overrightarrow{AB}} \boldsymbol{E} \cdot \mathrm{d}\boldsymbol{l}$ is the induced electromotive force of the conductor AB, $e_{DC} = \int_{\overrightarrow{DC}} \boldsymbol{E} \cdot \mathrm{d}\boldsymbol{l}$ is the induced electromotive force of the conductor DC, R_{DC} is the resistance of the conductor DC, L_{DC} is the inductance of the conductor DC, $M_{DC\text{-}YZ}$ is the mutual inductance between conductor DC and YZ. It should be noted that, since the inner conductor and outer conductor of the same coaxial cable have basically identical spatial form, the induced electromotive forces on them may be regarded as equal, it is $e_{AB} = e_{DC}$.

In this case, the signal after integration $v_{\mathrm{a}1}$, which is acquired by the oscilloscope may be expressed as

$$v_{\mathrm{a}1} = \frac{1}{T_1} \int v_{\mathrm{t}1} \mathrm{d}t = \frac{1}{T_1} \int v_{\mathrm{c}1} \mathrm{d}t + K_{\mathrm{I}} \tag{14}$$

where $\int v_{\mathrm{c}1} \mathrm{d}t / T_1$ is the integral of the Rogowski coil signal, i.e., the expected signal proportional to the measured current. The second term K_{I} in (13) is the component of the inductive coupling interference, which is

$$K_{\mathrm{I}} = -\frac{1}{T_1} \int \left[R_{DC} i + (L_{DC} - M_{DC\text{-}YZ}) \frac{\mathrm{d}i}{\mathrm{d}t}\right] \mathrm{d}t \tag{15}$$

Assuming the outer conductors of the two coaxial cables have the same resistance and inductance, the other signal acquired by the oscilloscope is

$$v_{\mathrm{a}2} = \frac{1}{T_1} \int v_{\mathrm{t}2} \mathrm{d}t = \frac{1}{T_1} \int v_{\mathrm{c}2} \mathrm{d}t - K_{\mathrm{I}}. \tag{16}$$

As shown in (14) and (16), for two Rogowski coils with CES, the measured current waveforms contain symmetrical inductive coupling interference components.

More than two cables will form multiple loops, thus producing multiple inductive coupling interference components that are superimposed on each signal. As seen in (13)–(16), the interference component is only related to the voltage drop caused by the induced current on the outer conductor of the coaxial cable. Therefore, when analyzing the effects of the inductive coupling on measurements, only the outer conductor needs to be modeled, as illustrated in Fig. 8.

Assuming that n coaxial cable outer conductors have the same resistance R_{b} and inductance L_{b}. The mutual inductance between branches is designated by their subscripts. The branch currents can be obtained through any circuit-solving method with the aforementioned approach. The voltage signals acquired

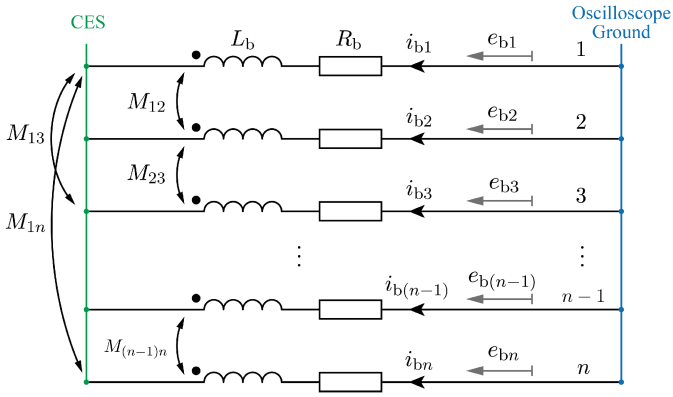

Fig. 8. Model of multiple Rogowski coils with CES.

by the oscilloscope are

$$\boldsymbol{v}_{\mathrm{a}} = \frac{1}{T_1} \int \boldsymbol{v}_{\mathrm{c}} \mathrm{d}t + \boldsymbol{K}_{\mathrm{I}} \tag{17}$$

where $\boldsymbol{v}_{\mathrm{a}} = [v_{\mathrm{a}1}, v_{\mathrm{a}2}, \ldots, v_{\mathrm{a}n}^{\top}$ is the column vector of the acquired signals, $\boldsymbol{v}_{\mathrm{c}} = [v_{\mathrm{c}1}, v_{\mathrm{c}2}, \ldots, v_{\mathrm{c}n}]^{\top}$ is the column vector of the output voltages of the Rogowski coils, and $\boldsymbol{K}_{\mathrm{I}}$ is the vector of the inductive coupling interference components, which is

$$\boldsymbol{K}_{\mathrm{I}} = -\frac{1}{T_1} \int \left(R_{\mathrm{b}} + \boldsymbol{L} \frac{\mathrm{d}}{\mathrm{d}t}\right) \boldsymbol{i}_{\mathrm{b}} \mathrm{d}t \tag{18}$$

where $\boldsymbol{i}_{\mathrm{b}} = [i_{\mathrm{b}1}, i_{\mathrm{b}2}, \ldots, i_{\mathrm{b}n}]^{\top}$ is the column vector of the conductor currents, and $\boldsymbol{L}$ is the symmetric inductance matrix as follows:

$$\boldsymbol{L} = \begin{bmatrix} L_{\mathrm{b}} & M_{12} & M_{13} & \cdots & M_{1n} \\ M_{21} & L_{\mathrm{b}} & M_{23} & \cdots & M_{2n} \\ M_{31} & M_{32} & L_{\mathrm{b}} & \cdots & M_{3n} \\ \vdots & \vdots & \vdots & \ddots & \vdots \\ M_{n1} & M_{n2} & M_{n3} & \cdots & L_{\mathrm{b}} \end{bmatrix}. \tag{19}$$

According to Kirchhoff's current law, the sum of all elements in the vector $\boldsymbol{i}_b$ is zero. Since integration and $(R_{\mathrm{b}} + \boldsymbol{L}\frac{\mathrm{d}}{\mathrm{d}t})$ in (18) are linear operators, the sum of all elements in the vector $\boldsymbol{K}_{\mathrm{I}}$ is also zero. This demonstrates that for more than two Rogowski coils with CES, there is still symmetry in the inductive coupling interference components.

In summary, the inductive coupling interference affects the measurement accuracy of PCB Rogowski coil arrays with CES. Therefore, corresponding suppression methods need to be proposed.

III. PCB Rogowski Coil Array With Discrete Electrostatic Shielding

As derived in the previous section, the inductive coupling interference is mainly related to the induced currents $\boldsymbol{i}_{\mathrm{b}}$ in (18). Therefore, in order to ensure the measurement accuracy of PCB Rogowski coil array, the induced currents must be eliminated. Magnetic flux passing through the loops may be minimized by braiding multiple coaxial cables in a stranded fashion, thereby

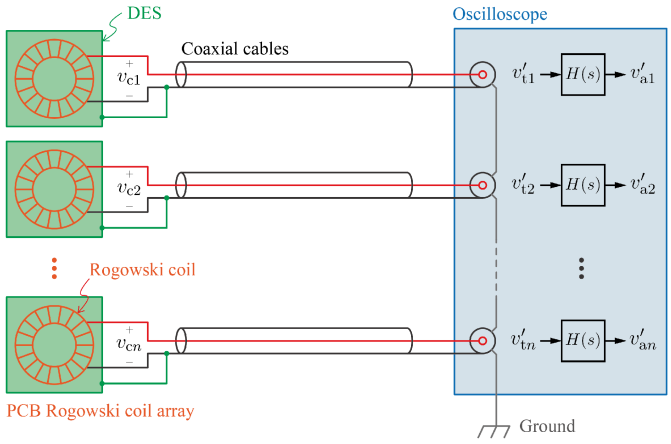

Fig. 9. Schematic diagram of the current measurement system with DES.

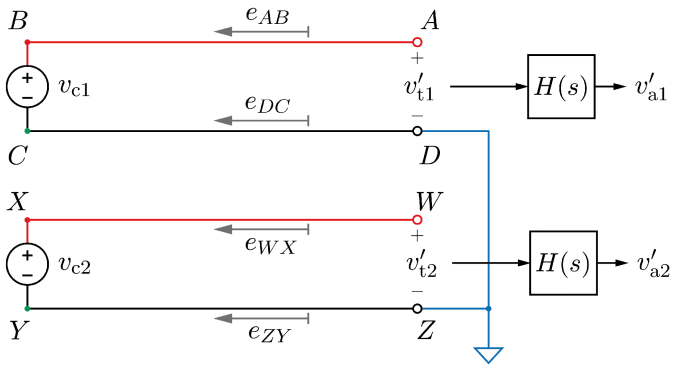

Fig. 10. Model of two Rogowski coils with DES.

reducing the amplitude of the interference components. However, this method cannot completely eliminate the inductive coupling.

This article proposes a PCB Rogowski coil array with DES. Fig. 9 illustrates the basic concept of the PCB Rogowski coil array with DES. Compared with the conventional CES structure in Fig. 4, the DES provides an independent electrostatic shielding for each Rogowski coil. The electrostatic shieldings of different coils are disconnected, avoiding the formation of loops. Therefore, in the PCB Rogowski coil array with DES, the induced currents from inductive coupling interference are identically zero.

The circuit model of two Rogowski coils with DES is shown in Fig. 10. Since there are no unexpected loops, no induced currents exist in the circuit as well. In this case, the voltage signal at the end of the coaxial cable v'_{t1} may be expressed as

$$\begin{aligned} v'_{\mathrm{t1}} &= \varphi_A - \varphi_D = (\varphi_B - e_{AB}) - (\varphi_C - e_{DC}) \\ &= (\varphi_B - \varphi_C) - (e_{AB} - e_{DC}) = v_{\mathrm{c1}} \end{aligned} \tag{20}$$

where $e_{AB} = e_{DC}$. This demonstrates that with DES, the signals on both ends of the coaxial cable are consistent. The signal v'_{a1} acquired by the oscilloscope is the integral of the coil signal v_{c1}

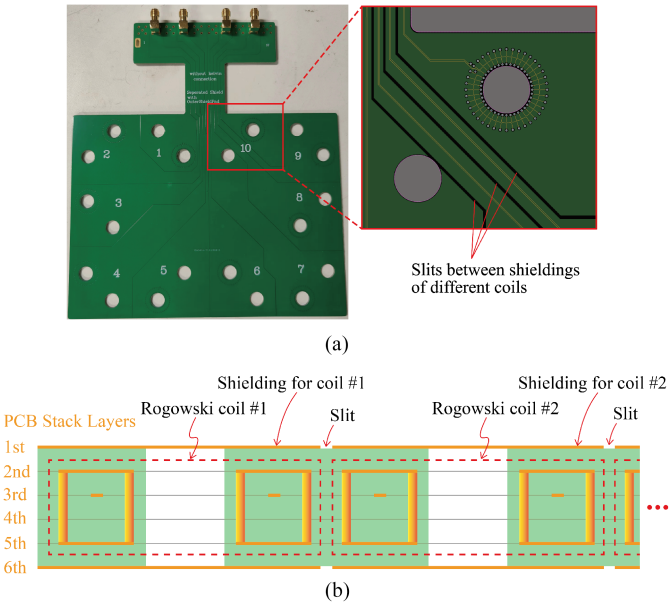

Fig. 11. PCB Rogowski coil array with DES. (a) Physical appearance. (b) Cross-sectional diagram.

as (21), and it is proportional to the measured current

$$v'_{\mathrm{a1}} = \frac{1}{T_1}\int v'_{\mathrm{t1}}\mathrm{d}t = \frac{1}{T_1}\int v_{\mathrm{c1}}\mathrm{d}t. \tag{21}$$

Similarly, for multiple coils equipped with DES, since there is no unexpected loop, $\boldsymbol{i}_{\mathrm{b}} = 0$ may be substituted into (16) and (17) to get $\boldsymbol{K}_{\mathrm{I}} = 0$ and

$$\boldsymbol{v}'_{\mathrm{a}} = \frac{1}{T_1}\int \boldsymbol{v}_{\mathrm{c}}\mathrm{d}t. \tag{22}$$

The signals acquired by the oscilloscope are exactly the integral of the coil signals. Therefore, PCB Rogowski coil arrays with DES are not affected by inductive coupling interference.

Fig. 11 shows the physical appearance and cross-sectional diagram of the PCB Rogowski coil array with DES. The top and bottom copper layers of the PCB are partitioned by slits into multiple sections corresponding to each coil. The shielding of each coil is connected to the outer conductor of the corresponding coaxial cable. Although the outer conductors of the coaxial cables are connected together at one end by the oscilloscope ground, the other ends are disconnected from each other, thus, avoiding formation of loops and associated inductive coupling interference.

IV. Verification and Discussion

Rogowski coils are modeled as mutual inductances in Section II. The validity of this model should be verified. The verification process is divided into two parts: determining the bandwidth of the current of the IGBT power device and measuring the frequency characteristics of the Rogowski coil. The total current of the IGBT power device in Fig. 2(d) is measured using a CWT MiniHF 6 coil (23 MHz bandwidth, 1.2 kA range) from PEM, and the resulting double-pulse current waveform is shown in Fig. 12(a). Performing a Fourier transform on this

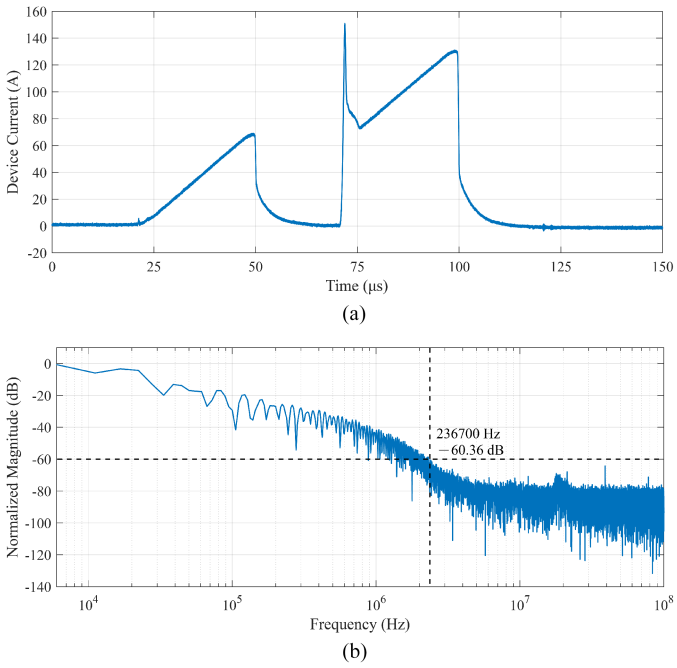

Fig. 12. Current characteristics of the IGBT power device. (a) Current waveform. (b) Normalized spectrum.

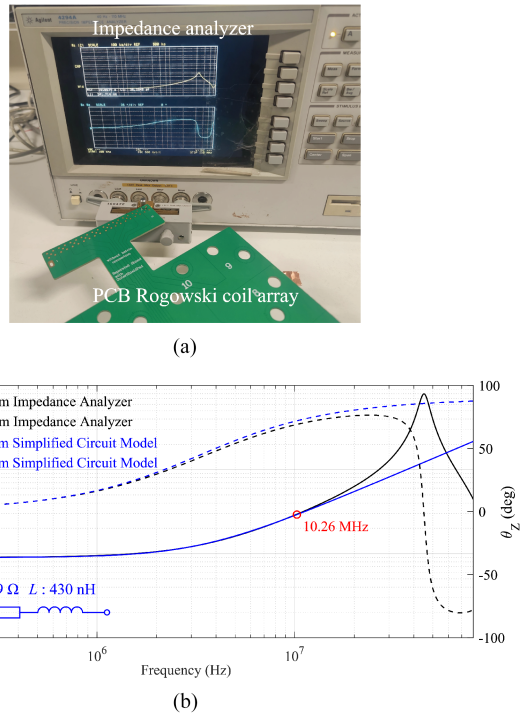

Fig. 13. Impedance characteristics of the PCB Rogowski coil. (a) Photo of the measurement process. (b) Impedance-frequency curves of the actual coil and the simplified model.

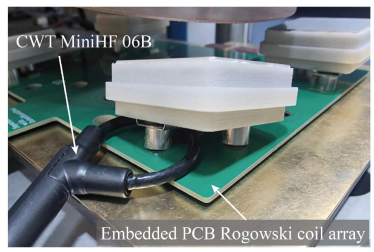

Fig. 14. Configuration of the sensitivity experiment.

current waveform, while normalizing it to the maximum value of the current amplitude, yields the signal spectrum shown in Fig. 12(b). From the cursor information, most of the signal components within the range of 0 dB to −60 dB are concentrated below 2.367 MHz. These signal components are already able to reconstruct the current waveform with high precision. Therefore, it can be considered that the signal bandwidth of the current of this IGBT power device is 2.5 MHz.

The impedance-frequency characteristics of a single Rogowski coil in the array is measured using 4294 A impedance analyzer (40 Hz to 110 MHz bandwidth) from Keysight. Fig. 13(b) shows the curves of the impedance magnitude and the phase angle of the Rogowski coil versus frequency. Comparing the curves from the impedance analyzer and from the simplified circuit model (by connecting a 9 Ω resistor and a 430 nH inductor in series), the difference in impedance magnitude is less than 1% and the difference in impedance angle is less than 3° when the signal frequency is lower than 10.26 MHz. Accordingly, the simplified circuit model in Fig. 13(b) is valid when measuring currents with a bandwidth of 2.5 MHz of the IGBT power device. In addition, the input resistance of the integrator (about 4 MΩ) is much larger than the resistance of the coil R (about 9 Ω). Therefore, a simple mutual inductance model as (1) can be used to accurately characterize the behavior of the Rogowski coils in the coil arrays when measuring the currents of the IGBT power device.

The manufacturing parameters of printed circuit board as well as the shape of the current-carrying conductor can affect the sensitivity of the PCB Rogowski current sensor. Therefore, before using the PCB Rogowski current sensor for the first time, it is good practice to conduct comparison experiments with commercial coils to determine its actual sensitivity. The experiment using a PCB Rogowski coil and a CWT MiniHF 06B coil (30 MHz bandwidth, 120 A range) to simultaneously measure the current of a single chip in the IGBT power device is shown in Fig. 14.

Fig. 15 shows the collector-emitter voltage v_{CE} and the gate-emitter voltage v_{GE} of the IGBT device, the single chip current i_{CWT} from the CWT coil, and the voltage signal v_{ROGO} from the PCB Rogowski current sensor during a double pulse test. The waveforms of i_{CWT} and v_{ROGO} are in high consistency, thus verifying the accuracy of the PCB Rogowski coils. The sensitivity of the PCB Rogowski current sensor can be calculated from the scale of the waveforms as 62.3 mV/A.

Experiments are then conducted to measure the internal current distribution of the IGBT power device using PCB Rogowski coil array with different shieldings. The double pulse test platform is shown in Fig. 16. The PCB Rogowski coils are connected to the integrators with coaxial cables, and the integrators are connected to an oscilloscope for signal acquisition. Fig. 17 plots the current waveforms measured by the Rogowski coil array with

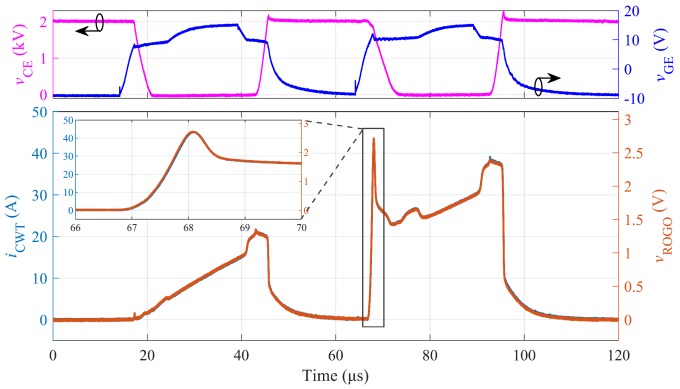

Fig. 15. Waveforms of the sensitivity experiment.

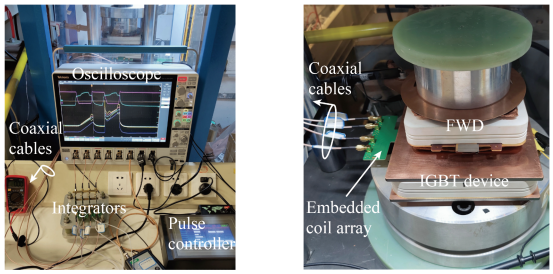

Fig. 16. Double pulse test platform. (a) Front view. (b) Mounting position of the device.

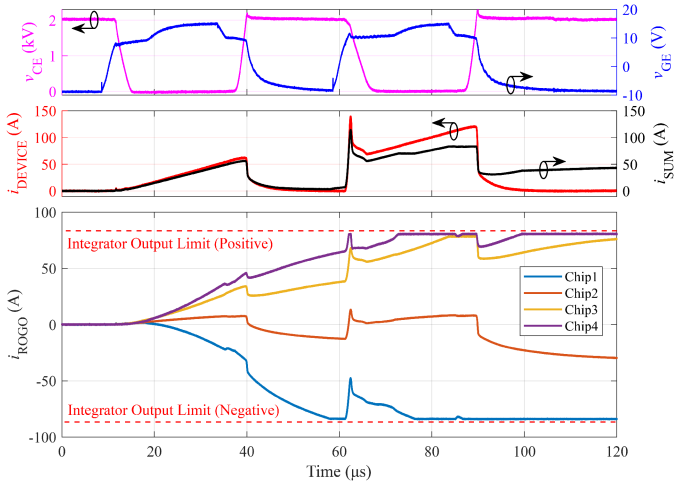

Fig. 17. Waveforms of the switching experiment while using the Rogowski coil array with CES.

CES during the double pulse test. In addition, the experiment provides a comparison between the sum of the four currents i_{SUM} measured by the PCB Rogowski coil array with CES and the total device current i_{DEVICE} measured by CWT MiniHF 6. After turn-ON of the first pulse, rapid waveform dispersion is observed, due to the impact of the inductive coupling interference. At this point, the i_{ROGO} measured by Rogowski coil do not represent the actual currents of the paralleled chips, but the superpositions of the currents and the inductive coupling interference components. Two noteworthy characteristics validate the theoretical analyses

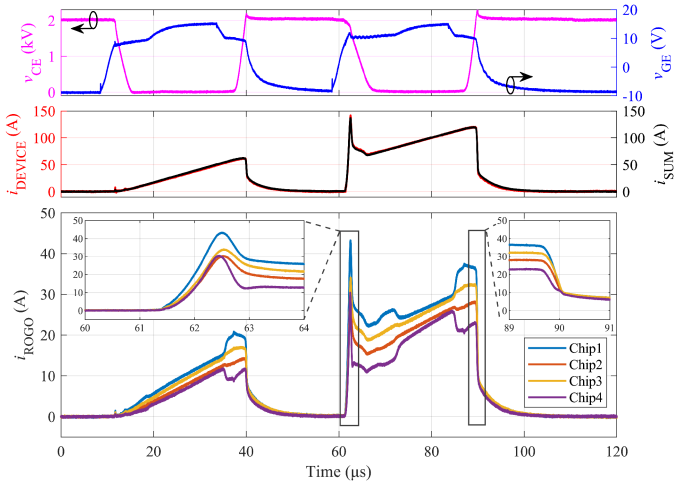

Fig. 18. Waveforms of the switching experiment while using the Rogowski coil array with DES.

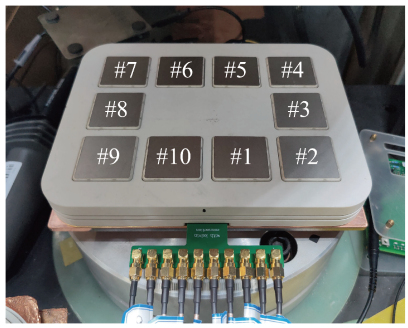

Fig. 19. Configuration of the 10-chip IGBT device.

in Section II. First, no dispersion arises prior to the pulses when no currents flow through the power device, since the power currents in the double pulse test circuit are the interference sources. Second, the sum of all dispersed waveforms remains approximately equal to the total device current before reaching integrator limits at 57 μs, this proves the symmetrical nature of the inductive coupling interference components.

The current waveforms measured by the Rogowski coil array with DES during a double pulse test are plotted in Fig. 18. The absence of the dispersion in current waveforms demonstrates the effectiveness of the DES structure to suppress inductive coupling interference. The consistent total current waveforms demonstrate the accuracy of the measurements by the Rogowski coil array with DES.

Furthermore, the PCB Rogowski coil array with DES is utilized to obtain the current distribution among ten paralleled chips inside an IGBT power device. The ten paralleled IGBT chips in the power device is shown in Fig. 19, with the numbers representing chip IDs. These chips have been screened and the threshold voltages range from 6.39 to 6.43 V. The measured current waveforms during the double pulse test are presented in Fig. 20. It may be observed that the turn-OFF current consistency among the paralleled chips is relatively better than the turn-ON. Fig. 21 maps the turn-ON current peak values of the paralleled chips according to their spatial positions. It is revealed that

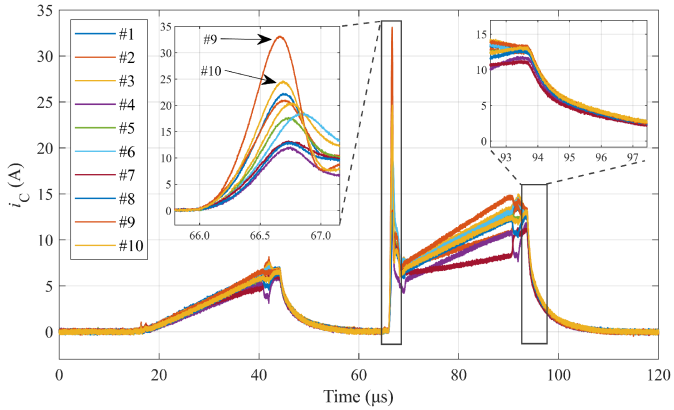

Fig. 20. Waveforms of the current distribution of the 10-chip IGBT device.

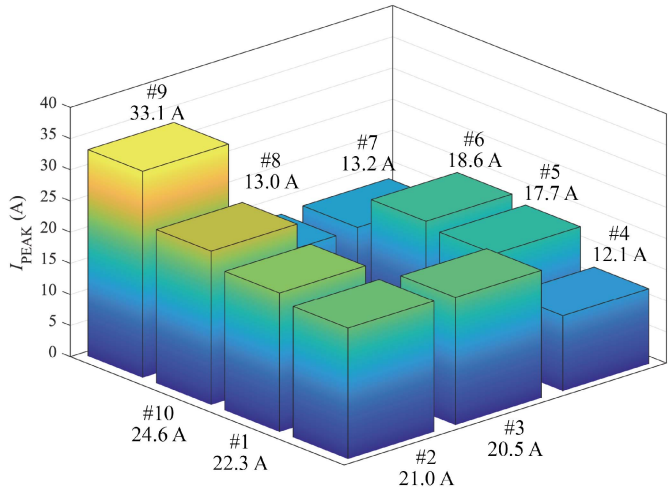

Fig. 21. Turn-ON current peaks against the corresponding spatial positions.

during the turn-ON transient, chip #9, #10, #1, and #2 flow relatively high currents. The current distribution of the chips is affected by a variety of factors, such as the characteristics of the chips, the parasitic parameters of the package, the mechanical stresses applied to the chips, the temperature of the chips, and so on [34]. Therefore, the current measurement enables opportunities to iteratively improve the design of the power device for more balanced current sharing among paralleled chips during transients.

V. Conclusion

This article proposes a PCB Rogowski coil array with discrete electrostatic shielding for measuring chip currents inside power devices, which is immune to both capacitive and inductive coupling interference. Conventional PCB Rogowski coil arrays with CES suffer from inductive coupling interference. The inductive coupling interference is caused by induced currents in the outer conductors of the coaxial cables. The sum of the inductive coupling interference components for all Rogowski coils is deduced to be zero. The waveforms measured by the PCB Rogowski coil array with continuous electrostatic shielding are observed to have symmetrical dispersion, which is caused by the aforementioned inductive coupling interference. The immunity to inductive coupling interference of the PCB Rogowski coil array with discrete electrostatic shielding is verified in another switching experiment. The PCB Rogowski coil array with discrete electrostatic shielding proposed in this article is applied to a 10-chip IGBT power device. The switching currents of the 10 paralleled chips are measured accurately, and the turn-ON transient current consistency is found to be worse than the turn-OFF transient current consistency. The relationship between the turn-ON current peaks and the positions of the paralleled chips in the IGBT power device is also presented. The PCB Rogowski coil array with discrete electrostatic shielding proposed in this article is an accurate current measurement tool for paralleled chips inside power devices, thus, providing a foundation for condition monitoring and design optimization of power devices.

References

[1] J. Lutz, H. Schlangenotto, U. Scheuermann, and R. D. Doncker, *Semiconductor Power Devices: Physics, Characteristics, Reliability*. New York, NY, USA: Springer, 2018.
[2] A. Volke and M. Hornkamp, *IGBT Modules: Technologies, Driver and Application*. Munich, Germany: Infineon Technologies AG, 2017.
[3] U. Schlapbach, "Dynamic paralleling problems in IGBT module construction and application," in *Proc. 6th Int. Conf. Integr. Power Electron. Syst.*, 2010, pp. 1–7.
[4] Y. Takahashi, T. Koga, H. Kirihata, and Y. Seki, "2.5 kV-100 A flat-packaged IGBT (micro-stack IGBT)," *IEEE Trans. Electron Devices*, vol. 43, no. 12, pp. 2276–2282, Dec. 1996.
[5] J. C. Joyce, "Current sharing and redistribution in high power IGBT modules," Ph.D. dissertation, Cambridge Univ. Eng. Dept., Univ. Cambridge, Cambridge, U.K., 2001.
[6] R. Letor, "Static and dynamic behavior of paralleled IGBTs," *IEEE Trans. Ind. Appl.*, vol. 28, no. 2, pp. 395–402, Mar./Apr. 1992.
[7] H. Li et al., "Influences of device and circuit mismatches on paralleling silicon carbide MOSFETs," *IEEE Trans. Power Electron.*, vol. 31, no. 1, pp. 621–634, Jan. 2016.
[8] Z. Zeng, X. Zhang, and X. Li, "Layout-dominated dynamic current imbalance in multichip power module: Mechanism modeling and comparative evaluation," *IEEE Trans. Power Electron.*, vol. 34, no. 11, pp. 11199–11214, Nov. 2019.
[9] L. Tinschert, A. R. Årdal, T. Poller, M. Bohlländer, M. Hernes, and J. Lutz, "Possible failure modes in press-pack IGBTs," *Microelectron. Rel.*, vol. 55, no. 6, pp. 903–911, 2015.
[10] M. Riccio, A. Castellazzi, G. D. Falco, and A. Irace, "Experimental analysis of electro-thermal instability in SiC power MOSFETs," *Microelectron. Rel.*, vol. 53, no. 9, pp. 1739–1744, 2013.
[11] A. J. L. Joannou, D. C. Pentz, J. D. van Wyk, and A. S. de Beer, "Some considerations for miniaturized measurement shunts in high frequency power electronic converters," in *Proc. 16th Eur. Conf. Power Electron. Appl.*, 2014, pp. 1–7.
[12] J. Ferreira, W. Cronje, and W. Relihan, "Integration of high frequency current shunts in power electronic circuits," *IEEE Trans. Power Electron.*, vol. 10, no. 1, pp. 32–37, Jan. 1995.
[13] L. Dalessandro, N. Karrer, and J. W. Kolar, "High-performance planar isolated current sensor for power electronics applications," *IEEE Trans. Power Electron.*, vol. 22, no. 5, pp. 1682–1692, Sep. 2007.
[14] E. Ramsden, *Hall-Effect Sensors: Theory and Application*, 2nd ed. Burlington, MA, USA: Newnes, 2006.
[15] C. Xu, J.-G. Liu, Q. Zhang, C. Xu, and Y. Yang, "Investigation of the thermal drift of open-loop Hall effect current sensor and its improvement," in *Proc. IEEE Int. Workshop Appl. Meas. Power Syst.*, 2015, pp. 19–24.
[16] Z. Xin, H. Li, Q. Liu, and P. C. Loh, "A review of megahertz current sensors for megahertz power converters," *IEEE Trans. Power Electron.*, vol. 37, no. 6, pp. 6720–6738, Jun. 2022.
[17] Q. Xu et al., "Design of PCB Rogowski coil current sensor with low droop distortion," *IEEE Trans. Power Electron.*, vol. 38, no. 4, pp. 5513–5523, Apr. 2023.

[18] M. H. Samimi, A. Mahari, M. A. Farahnakian, and H. Mohseni, "The Rogowski coil principles and applications: A review," *IEEE Sensors J.*, vol. 15, no. 2, pp. 651–658, Feb. 2015.
[19] W. Ray and R. Davis, "Wide bandwidth Rogowski current transducers," *EPE J.*, vol. 3, no. 1, pp. 51–59, Mar. 1993.
[20] P. Palmer, B. Stark, and J. Joyce, "Noninvasive measurement of chip currents in IGBT modules," in *Proc. Rec. 28th Annu. IEEE Power Electron. Specialists Conf.*, 1997, vol. 1, pp. 166–171.
[21] M. Furuya and Y. Ishiyama, "Current measurement inside press pack IGBTs," *Fuji Electric J.*, vol. 75, no. 8, pp. 1–3, 2002.
[22] Y. Shi, Z. Xin, P. C. Loh, and F. Blaabjerg, "A review of traditional helical to recent miniaturized printed circuit board Rogowski coils for power-electronic applications," *IEEE Trans. Power Electron.*, vol. 35, no. 11, pp. 12207–12222, Nov. 2020.
[23] C. Jiao, J. Zhang, Z. Zhao, Z. Zhang, and Y. Fan, "Research on small square PCB Rogowski coil measuring transient current in the power electronics devices," *Sensors*, vol. 19, no. 1919, Jan. 2019, Art. no. 4176.
[24] D. Gerber, T. Guillod, R. Leutwyler, and J. Biela, "Gate unit with improved short-circuit detection and turn-off capability for 4.5-kV press-pack IGBTs operated at 4-kA pulse current," *IEEE Plasma Sci.*, vol. 41, no. 10, pp. 2641–2648, Oct. 2013.
[25] M. Tsukuda, M. Koga, K. Nakashima, and I. Omura, "Micro PCB Rogowski coil for current monitoring and protection of high voltage power modules," *Microelectron. Rel.*, vol. 64, pp. 479–483, Sep. 2016.
[26] S. Fu et al., "Current measurement method of multiple chips using rectangular PCB Rogowski coils integrated in press pack IGBT device," *IEEE Trans. Power Electron.*, vol. 38, no. 1, pp. 96–100, Jan. 2023.
[27] S. Fu, E. Deng, C. Peng, G. Zhang, Z. Zhao, and X. Cui, "Method of turns arrangement of noncircular Rogowski coil with rectangular section," *IEEE Trans. Instrum. Meas.*, vol. 70, 2021, Art. no. 9000310.
[28] S. Fu, "Research on current measurement method and application of paralleled chips inside press-packed IGBT device," Ph.D., North China Electric Power Univ., 2023.
[29] C. Peng, X. Li, M. Gu, Z. Zhao, X. Tang, and X. Cui, "Error analysis and improvement method of Rogowski coil in current measurement of internal chips in press-pack IGBT devices," *Proc. CSEE*, vol. 40, no. 22, pp. 7388–7398, 2020.
[30] C. Hewson and J. Aberdeen, "An improved Rogowski coil configuration for a high speed, compact current sensor with high immunity to voltage transients," in *Proc. IEEE Appl. Power Electron. Conf. Expo.*, 2018, pp. 571–578.
[31] P. Sun, X. Cui, S. Huang, P. Lai, Z. Zhao, and Z. Chen, "LTCC based current sensor for silicon carbide power module integration," *IEEE Trans. Power Electron.*, vol. 37, no. 2, pp. 1605–1614, Feb. 2022.
[32] J. Wang, Z. Shen, R. Burgos, and D. Boroyevich, "Integrated switch current sensor for short circuit protection and current control of 1.7-kV SiC MOSFET modules," in *Proc. IEEE Energy Convers. Congr. Expo.*, 2016, pp. 1–7.
[33] X. Cui, "Magnetic field and inductance of filament conductor segment model with current continuity," *Acta Physica Sinica*, vol. 69, no. 3, 2020, Art. no. 034101.
[34] C. Peng, X. Li, J. Fan, Z. Zhao, X. Tang, and X. Cui, "Experimental investigations on current sharing characteristics of parallel chips inside press-pack IGBT devices," *IEEE Trans. Power Electron.*, vol. 37, no. 9, pp. 10672–10680, Sep. 2022.

Yongfan Zhan was born in Hunan, China, in 1999. He received the B.Sc. degree in electrical engineering from North China Electric Power University, Baoding, China, in 2020. He is currently working toward the Ph.D. degree in electrical engineering with North China Electric Power University and Huairou Laboratory, Beijing, China.

His main research interests include the Rogowski current sensors and the packaging of high-power electronic devices.

Ganyu Feng was born in Hubei, China, in 1998. He received the B.Sc. degree in electrical engineering from China Three Gorges University, Hubei, China, in 2021. He is currently working toward the Ph.D. degree in electrical engineering with the State Key Laboratory of Alternate Electrical Power System with Renewable Energy Sources, North China Electric Power University, Baoding, China.

His main research interests include the packaging and reliability of high-voltage and high-power electronic devices.

Jia Wan was born in Jiangsu, China, in 1999. She received the B.Sc. degree in electrical engineering in 2021 from North China Electric Power University, Beijing, China, where she is currently working toward the postgraduate degree in electrical engineering with the State Key Laboratory of Alternate Electrical Power System with Renewable Energy Sources.

Her main research interest includes the Rogowski current sensors.

Xuebao Li (Member, IEEE) was born in Tianjin, China, in 1988. He received the B.Sc. and Ph.D. degrees in electrical engineering from North China Electric Power University, Beijing, China, in 2011 and 2016, respectively.

He is currently an Associate Professor with the State Key Laboratory of Alternate Electrical Power System with Renewable Energy Sources, North China Electric Power University, Beijing, China, and a Scientist with Huairou Laboratory, Beijing, China. His research interests include the electromagnetics environment and electromagnetic compatibility in power systems, and insulation problems in high-voltage apparatus.

Rui Jin (Member, IEEE) was born in Liaoning, China, in 1982. She received the Ph.D. degree in physics from Imperial College London, London, U.K., in 2009.

She is currently the Director of the Power Semiconductor Research Institute, Beijing Institute of Smart Energy, Beijing, China, and a Scientist with Huairou Laboratory, Beijing, China. Her main research interests include the design and fabrication of high-power electronic devices.

Prof. Jin is a Fellow of the IEEE PES Technical Committee on Transmission and the Deputy Secretary-General of China IGBT Technology Innovation and Industry Alliance.

Peng Sun was born in Jilin, China, in 1994. He received the bachelor's and Ph.D. degrees in electrical engineering from North China Electric Power University, Beijing, China, in 2016 and 2022, respectively.

He worked as Visiting Scholar with the University of Arkansas, Fayetteville, AR, USA from 2019 to 2020. Currently, he is working as a Lecturer with the State Key Laboratory of Alternate Electrical Power System with Renewable Energy Sources, North China Electric Power University. His research interests include the packaging, condition monitoring, and reliability of power electronics devices.

Zhibin Zhao (Member, IEEE) was born in Hebei, China, in 1977. He received the Ph.D. degree in electrical engineering from North China Electric Power University, Baoding, China, in 2005.

He is currently a Professor with the State Key Laboratory of Alternate Electrical Power System with Renewable Energy Sources, North China Electric Power University, Beijing, China, and a Scientist with Huairou Laboratory, Beijing, China. His main research interests include computational electromagnetics and electromagnetic compatibility in high-power electronic devices.

Xiang Cui (Senior Member, IEEE) was born in Baoding, Hebei, China, in 1960. He received the B.Sc. and M.Sc. degrees in electrical engineering from North China Electric Power University, Baoding, China, in 1982 and 1984, respectively, and the Ph.D. degree in accelerator physics from the China Institute of Atomic Energy, Beijing, China, in 1988.

He is currently a Professor with the State Key Laboratory of Alternate Electrical Power System with Renewable Energy Sources, North China Electric Power University and a Scientist of Huairou Laboratory. His research interests include electromagnetics, high-voltage apparatus, and high-power electronic devices.

Prof. Cui is a Fellow of the Chinese Society for Electrical Engineering and the China Electrotechnical Society.